Journal of Molecular Catalysis A: Chemical 323 (2010) 70–77

Contents lists available at ScienceDirect

Journal of Molecular Catalysis A: Chemical

journal homepage: www.elsevier.com/locate/molcata

TiO_2–SiO_2 mixed oxide supported MoO_3 catalyst: Physicochemical characterization and activities in nitration of phenol

S.M. Kemdeo [a], V.S. Sapkal [b], G.N. Chaudhari [a,*]

[a] Department of Chemistry, Shri Shivaji Science College, Amravati, Maharashtra 444601, India
[b] University Department of Chemical Technology, SGB Amravati University, Amravati, India

ARTICLE INFO

Article history:
Received 14 January 2010
Received in revised form 11 March 2010
Accepted 12 March 2010
Available online 17 March 2010

Keywords:
MoO_3/TiO_2–SiO_2
TiO_2–SiO_2
NH_3-TPD
Nitration
o-Nitrophenol

ABSTRACT

12 wt% MoO_3/TiO_2–SiO_2 solid acid catalyst was prepared and calcined at various temperatures. The calcined catalyst was characterized by XRD, FT-IR, BET, SEM, NH_3-TPD and pyridine adsorbed FT-IR methods. The effect of calcination temperature on activity of catalyst was studied by choosing liquid phase nitration of phenol as a model reaction. For the same reaction effect of various solvents, effect of reaction time and reusability of the catalyst was also studied. Catalyst calcined at 500 °C temperature showed highest phenol conversion whereas greater o-nitrophenol selectivity is claimed over catalyst calcined at 700 °C. It was observed that high phenol conversion co-relates with the presence of greater number of strong Brönsted acid sites over the catalyst surface whereas the selectivity of o-nitrophenol is related to the pore size of the catalysts. No use of sulfuric acid along with the nitric acid used in its diluted form in the reaction makes the process safe and environmentally friendly.

1. Introduction

Nitration of aromatic compound is widely used in organic syntheses and industrial application. Among the various nitroaromatic compounds nitrophenols are important intermediate as they are greatly utilizable in synthesis of drugs, pharmaceuticals, dyestuff, perfumes, plastics and explosives [1]. Earlier industrial nitration processes involve the use of nitric acid and sulfuric acid mixtures (liquid phase) which are responsible for the major difficulties like corrosion of processing equipments and generation of large amount of hazardous waste [1,2]. Therefore lots of efforts had been directed to seek environmentally friendly and reusable alternatives for such acid combination in recent year. Nitration using solid acid may be answer to these problems as solid acid effectively plays the role of sulfuric acid in the reaction, assisting the formation of nitronium ions. Dedicated to above issue, many researchers tried nitration of phenol using $AcONO_2/HNO_3$ [3], $TfONO_2$ [4], N_2O_4 [5] and *N*-nitropyrazole/BF_3 [6]. Recently the nitration of phenol has been attempted also on zeolites [7,8] modified silica [9], sulfated zirconia [10], Mo/SiO_2, H-Y, H-Beta and other solid acid catalysts [11].

Concentrating upon regioselectivity, La (NO_3) as a catalyst in the presence of hydrochloric acid gives *o*/*p* ratio of 2.1 when phenol is nitrated in water–ether system at room temperature [12]. Moreover, catalyst suspended in acetonitrile and treated with nitronium tetrafluroborate was also come up as excellent formulation in favor of good *o*/*p* nitrophenol ratio [13]. But instability of active phase and tedious workup procedures with these catalysts demands high regioselective catalyst operable with simpler workup procedure in nitration of phenol.

MoO_3 supported on TiO_2 is reported as excellent catalyst for the selective oxidation of hydrocarbon [14], selective catalytic reduction of NO_x by ammonia [15], alkene metathesis [16] and sulfided hydrodesulfurization [17]. MoO_3/SiO_2 is another candidate successfully tested for selective catalytic oxidation of ammonia to N_2 and the direct conversion of methane to methanol [18,19]. Their performance is also well known for transestrification of dimethyl oxalate with phenol and nitration of benzene [20,21].

The type of support plays an important role on the catalytic properties and for a given reaction the activity and selectivity of the catalyst can be improved by the use of an appropriate support [22]. Thus intrinsic being characteristics of both titania and silica support can be explored fully by using them in combination. Therefore the combined TiO_2–SiO_2 mixed oxide has attracted much attention recently as a support [23–25].

In this context, we strive to introduce TiO_2–SiO_2 mixed oxide supported MoO_3 solid acid catalyst for nitration reaction of phenol in the hope of avoiding the use of large volume of sulfuric acid and adjusting the isomer proportion of nitrophenol in order to meet the desired markets. This solid acid is also expected to offer significant industrial benefits due to the simpler work up procedure, easy sep-

* Corresponding author.
E-mail address: nano.d@rediffmail.com (G.N. Chaudhari).

1381-1169/$ – see front matter © 2010 Elsevier B.V. All rights reserved.
doi:10.1016/j.molcata.2010.03.017

aration of catalyst, the nature of non-corrosiveness and superior recycling.

Therefore in the present investigation 1:1 mole ratio TiO_2–SiO_2 mixed oxide support obtained via co-precipitation method was impregnated with 12 wt% MoO_3 using ammonium heptamolybdate and subjected to thermal treatment at various temperatures in order to understand the dispersion and its subsequent effect on the activity of catalyst. In this study thermal effects are examined by different characterization techniques including XRD, FT-IR, SEM, BET surface area, NH_3-TPD and pyridine adsorbed FT-IR and activities of the catalysts are monitored by choosing nitration of phenol as a model reaction.

2. Experimental

2.1. Catalyst preparation

1:1 mole ratio of TiO_2–SiO_2 mixed oxide support was prepared by co-precipitation method using ammonia as a precipitating agent [26]. Appropriate amount of cold $TiCl_4$ (Loba chemi, AR grade) was initially digested in cold conc. HCl and then diluted with doubly distilled water. To this aqueous solution the required quantity of Na_2SiO_3 (Loba chemi, AR grade) dissolved separately in deionized water was added, excess ammonia solution (25%) was also added to this mixture solution for better control of pH 8 and heated to 115 °C with vigorous stirring. Instantly a white precipitate formed in the solution is stirred for 6 h additionally and the precipitate was allowed to stand at room temperature for 24 h to facilitate the aging. The precipitate thus obtained was filtered off and thoroughly washed with deionized water until no chloride ion could be detected with $AgNO_3$ in the filtrate. The obtained sample was then oven dried at 120 °C for 16 h and finally calcined at 500 °C for 6 h in an open air atmosphere.

Molybdena (12 wt%) was deposited on 1:1 mole ratio of TiO_2–SiO_2 mixed oxide support by adopting incipient wetness method. To impregnate MoO_3, calculated amount of ammonium heptamolybdate was dissolved in doubly distilled water and few drops of dilute NH_4OH were added to make the solution clear and to keep pH constant (pH 8). Finally, powdered calcined support was then added to this solution and the excess of water was evaporated on water bath with continuous stirring. The resultant solid is then dried at 110 °C for 12 h, part of the obtained catalyst powder is again calcined at 500, 600, and 700 °C for 5 h.

For the simplicity in discussion, catalyst with 12 wt%MoO_3 supported on TiO_2–SiO_2 mixed oxide support, calcined at 500, 600, and 700 °C are coded as MTS-5, MTS-6, and MTS-7, respectively and commonly referred as 'Series of MTS catalysts'.

2.2. Catalyst characterization

XRD analysis was carried out with Phillips Holland, XRD system, PW1710 Using Cu-k_α (1.54056 Å) radiation, the diffractograms were recorded in 10–60° range of 2θ. The XRD phases present in the samples were identified with the help of JCPDS card files. Fourier transform infrared spectroscopy (FT-IR) spectra were recorded on Perkin-Elmer 1720 single beam spectrometer at ambient conditions using KBr disks, with a nominal resolution of 4 cm^{-1}. The mixed samples were pressed into a 10 mg/cm^2 self-supporting wafers before measurements were conducted at room temperature in the range of 1500–400 cm^{-1}. Temperature programmed desorption of ammonia (NH_3-TPD) was carried out using Micromeritics Autochem 2920 instrument. Scanning Electron Micrograms (SEM) was obtained using Instrument, JEOL JSM-6380. BET surface area and pore size was estimated by, Quantachrome Autosorb Automated Gas Sorption System, using N_2 as a probe molecule. Gas chromatograms were recorded on Perkin-Elmer Autosystem XL, with PE-1 column.

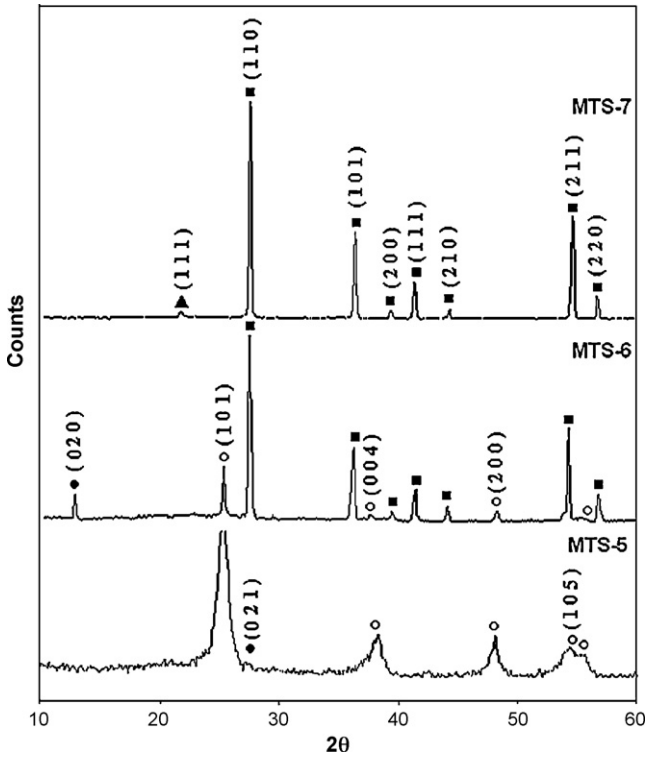

Fig. 1. XRD pattern of calcined samples: (○) lines due to anatase phase; (■) rutile phase of TiO_2; (●) MoO_3 and (▲) SiO_2.

2.3. Nitration of phenol

Liquid phase, batch process nitration of phenol was carried out at atmospheric pressure, using series of MTS catalysts, according to the procedure described elsewhere [11]. In the particular experiment, 2 g of phenol was taken in a round bottom flask containing 3 ml of solvent to which 1 g of catalyst pre-dried at 110 °C and 4 ml of 30% nitric acid were added and the reaction mixture was stirred at room temperature. After the completion of reaction catalyst was filtered off and products were extracted with diethyl ether and analyzed offline by gas chromatography and identified by their GC-retention times.

3. Results and discussion

3.1. Surface study of catalysts

3.1.1. XRD measurements

Powder XRD patterns of 12 wt% MoO_3/TiO_2–SiO_2 catalyst calcined at different temperature are shown in Fig. 1. At lower calcination temperature (500 °C) i.e. for MTS-5 catalyst, a broad peak due to anatase phase of TiO_2 (JCPDS File No. 21-1272) and peak of negligible intensity due to (0 2 1) plane of MoO_3 at d = 3.26 (JCPDS File No. 5-508) was observed. This suggests the monolayer accumulation of molybdena over TiO_2–SiO_2 mixed oxide support. The observation also indicates that MoO_3 phase is present in highly dispersed or amorphous state on the surface of support material. With increase in calcination temperature corresponding increase in crystallinity of anatase phases is seen and partial transformation of TiO_2 anatase in to TiO_2 rutile (JCPDS File No. 21-1276) phases starts, along with this, small peak attributed to MoO_3 (0 2 0) crystalline phase is observed due to structural rearrangements of the solid cat-

alyst. Therefore it can be concluded that amorphous TiO_2 enhances the association between MoO_3 and SiO_2 and improve the dispersion capacity of MoO_3 on the surface of SiO_2 whereas crystalline TiO_2 may not effectively contribute further to the interaction of MoO_3 with SiO_2. The above experimental observation also agrees with the assumptions of monolayer dispersion theory [27], according to which, amorphously dispersed TiO_2 has a much stronger interaction with the SiO_2 support and other metal oxides than crystalline TiO_2. At high temperature the interaction of MoO_3 with support weakens which causes three-dimensional oxide agglomerations; due to which MoO_3 exists over the surface of MTS-6 catalyst in its crystalline form. At calcination temperature of 700 °C, XRD lines due to rutile phase become very strong with no indication of any anatase phase. Thus, a complete transformation of anatase into rutile can be noted at this temperature. Moreover very new peak in diffractogram of MTS-7 corresponds to (1 0 1) plane of SiO_2 (JCPDS File No. 11-695) at $2\theta = 21.910°$ provides an additional evidence for lowered interaction of MoO_3 and TiO_2 with SiO_2. Because of its closer melting point (MoO_3, m.p. = 795 °C) to calcination temperature of catalyst (700 °C), MoO_3 is expected to be present as a spread layer over the support species or crystallite exist may be of size less than 4 nm (beyond the detection capacity of XRD technique) hence, no any peaks were observed due to MoO_3 phase in diffractogram of MTS-7 catalyst.

Experimental results revealed that calcination temperature is an important factor in anatase-to-rutile phase transformation. Generally the anatase-to-rutile phase transformation of impurity free TiO_2 occurs at 400 °C (673 K) and above temperatures [28]. Therefore from the XRD results of 12 wt% MoO_3/TiO_2–SiO_2 catalyst calcined at different temperatures it can be inferred that, presence of SiO_2 with TiO_2 inhibits the anatase-to-rutile phase transformation and secondly, at higher temperature the lowered interaction of rutile phase and MoO_3 with SiO_2 phase separates some SiO_2 species from TiO_2–SiO_2 matrix.

3.1.2. FT-IR

In order to get detailed information about the surface structure through the modes of vibration offered by different species on the surface of catalyst, FT-IR spectroscopic analysis of 12 wt% MoO_3/TiO_2–SiO_2 catalysts were done and results are displayed in Fig. 2. Generally the IR band at 1097 and 467 cm^{-1} corresponds to asymmetric stretching and bending modes of Si–O–Si linkage, respectively [29,30]. Whereas anatase and rutile phase exhibit the bands in 850–650 and 800–600 cm^{-1} region, respectively [31]. The Ti–O–Si infrared vibration is generally observed between 910 and 960 cm^{-1} [32,33] with the exact band position depending on the chemical composition of the sample as well as calibration and resolution of the instrument whereas terminal M=O stretch of MoO_3 phase can be identified from a band at 1000 cm^{-1} [31,34,35].

For the catalyst calcined at 500 °C (MTS-5) a prominent band appeared at 1101 cm^{-1} that corresponds to Si–O–Si linear stretch in SiO_2 and another band at 987 cm^{-1} is related to stretching vibration mode of M=O due to impregnated MoO_3 phase. The IR band at 929 cm^{-1} is assigned to Ti–O–Si species which clearly indicates the union of TiO_2 and SiO_2 counterparts of support material and the TiO_2 anatase phase can be detected from the IR band at 782 cm^{-1}.

Increase in calcination temperature brings out some modification in IR spectra of corresponding samples (MTS-6, MTS-7) because

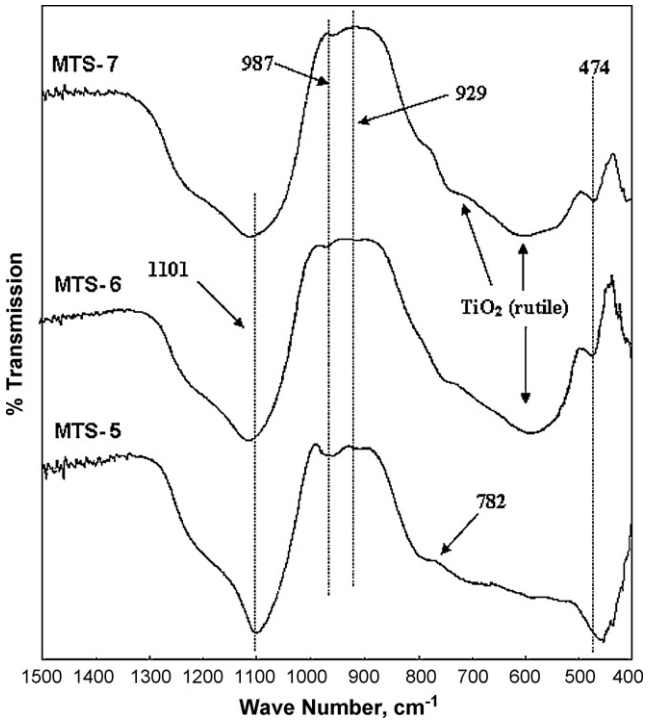

Fig. 2. FT-IR spectra of MTS series of catalyst samples.

of the structural reordering of the solids. In this regard, lowering of the intensity of band attributed to Ti–O–Si, upraise of new bands in the region 800–550 cm^{-1} and around 474 cm^{-1} and broadening of band at 1101 cm^{-1} can be seen. This happening is correlated to the formation of Ti–O–Ti and Si–O–Si bonds due to breakage of Ti–O–Si bonds at high temperature. This experimental observation is similar to the conclusions made by Gunji et al. [36] in his investigation regarding the thermal stability of Ti–O–Si structure. The fall in the intensity of the band at 987 cm^{-1} with progress in calcination temperature is seen which may be because of the increase in mutual interaction of molybdena with TiO_2 phase. Moreover the dominant existence of TiO_2 rutile phase over the catalyst surface might have masked the band corresponds to molybdena. The present IR results also show the evidence for phase transformation of titania anatase into rutile with progress in calcination temperature of catalyst hence, all these observations are inline with the XRD results.

3.1.3. BET surface area and pore size

TiO_2–SiO_2 mixed oxide support having N_2 BET surface area of 218 m^2/g was impregnated with 12 wt% MoO_3 using calculated amount of ammonium heptamolybdate and the corresponding results of BET surface area, pore volume and pore size of 12 wt% MoO_3/TiO_2–SiO_2 catalyst calcined at different temperature are summarized in Table 1. As soon as the TiO_2–SiO_2 support is impregnated with MoO_3 and subsequently activated at 500 °C, the drastic decrease in surface area for MTS-5 (106 m^2/g) sample was noted due to penetration of the active component into the pores of the support. Further progress in calcination temperature of catalyst up

Table 1
Surface area and acidity measurement of the catalysts.

Catalyst	Surface area (m^2/g)	Average pore diameter (Å)	Average pore volume (cm^3/g)	Amount of NH_3 desorbed (mmol/g)
MTS-5	106	68.52	0.1817	6.440
MTS-6	39	26.69	0.0268	0.901
MTS-7	15	13.03	0.0051	0.074

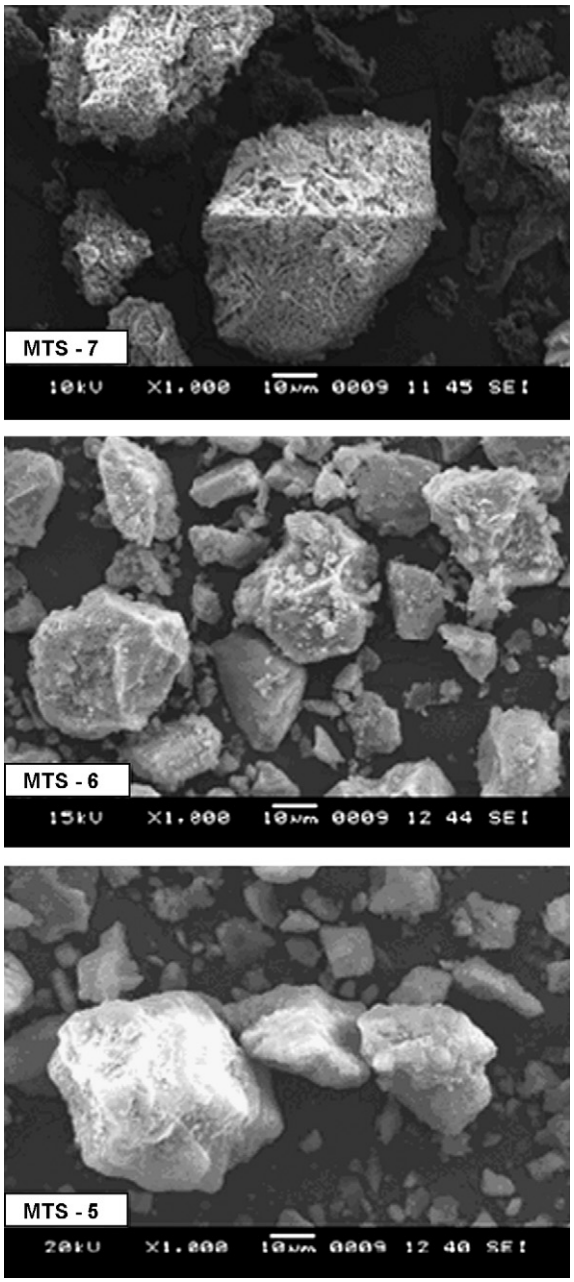

Fig. 3. Scanning Electron Micrographs of MTS series of catalysts.

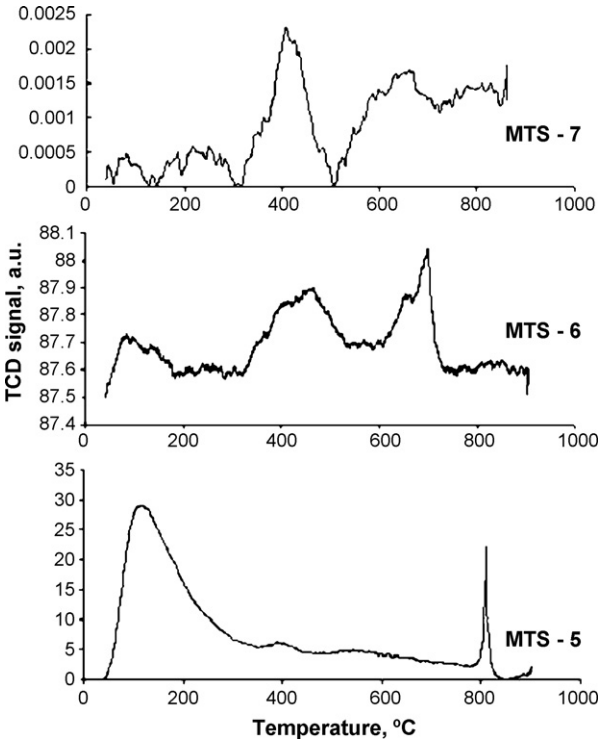

Fig. 4. NH_3-TPD profiles for samples: MTS-5, MTS-6 and MTS-7.

to 700 °C indicated the rapid fall in surface area (MTS-7 = 15 m^2/g) as well as the reduction in pore volume and pore diameter. This is mainly due to phase transformation of the titania anatase into rutile which is accelerated by calcination temperature. The calcination of catalyst at high temperature induces the crystalline growth in catalyst that results in to a formation of a denser solid material with narrow channels. Hence catalyst calcined at progressive temperature indicated the gradual loss in pore volume and pore size, intern in surface area.

3.1.4. SEM

Fig. 3 represents the results of scanning electron micrograms (SEM) recorded in order to demonstrate the morphology and particle size of the catalysts. As can be seen, with progress of calcination temperature, agglomerates are formed due to mutual interaction of small crystallites of the catalyst so the average particle size of catalyst MTS-5 was shifted from 15–25 to >30 μm for MTS-7. Beside this, the surface of MTS-7 catalyst appears to be sintered and reduced indicating the effect of higher calcination temperature (700 °C) on morphology of the catalyst. SEM result provides the back up to the trend observed in surface area measurements.

3.1.5. Ammonia desorption

MoO_3/TiO_2–SiO_2 catalyst calcined at various temperatures were subjected to temperature programmed desorption of ammonia (NH_3-TPD) to survey the acid amount and acid strength of catalysts. In NH_3-TPD profile, peaks are generally distributed into two regions, high temperature (HT) region (T > 400 °C) and low temperature (LT) region (T < 400 °C). Peaks in high temperature (HT) region are ascribed to desorption of ammonia from strong Brönsted and Lewis acid sites, while peaks in low temperature region are assigned to desorption of ammonia from weak acid sites [37,38]. NH_3-TPD profiles for the samples are shown in Fig. 4 and amount of ammonia desorbed is given in Table 1.

MTS-5 (6.44 mmol/g) has highest acidity among all MTS series of catalysts. NH_3-TPD profile for sample MTS-5 suggests the availability of greater number of weak acid sites as maxima of the broad ammonia desorption peak is centered at temperature 114 °C in LT region whereas another strong peak in HT region at 810 °C indicates the presence of strong acid sites as well. So, weak acid sites contribute mainly in total acid amount of MTS-5 sample. Weak acid sites are generally associated with terminal hydroxyl (–OH) groups of support and presence of Si–O–Ti species in TiO_2–SiO_2 matrix [39]. Rise in calcination temperature cause dehydroxylation of the surface and reduces the relative abundance of Si–O–Ti due to breaking of Ti–O–Si species in to Ti–O–Ti and Si–O–Si individual structures which results in to decrease in weak acid sites from the catalyst surface. Beside that, TiO_2 rutile crystallites formed (as evident from XRD and FT-IR analysis) exhibits strong Lewis acidity only [40]. Inline with this justification, sample MTS-6 showed lowered acidity (0.9017 mmol/g) as compared to that of MTS-5. At calcination temperature 700 °C, the above phenomenon becomes more severe

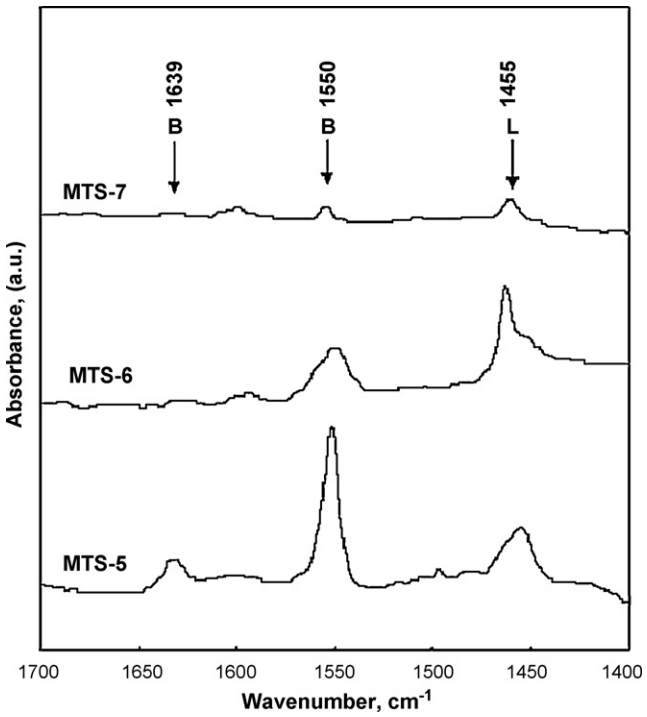

Fig. 5. FT-IR spectra of pyridine adsorbed catalyst samples (B = Brönsted, L = Lewis).

hence very low acidity is recorded for MTS-7 (0.074 mmol/g) catalyst.

With increase in calcination temperature of catalyst from 500 to 700 °C, peak maxima of NH_3-TPD profile shifts from 810 °C for MTS-5 to 409 °C for MTS-7. This clearly indicates the effect of calcination temperature on strong acidity over the catalyst surface. Strong acid sites in HT region are attributed to strong Brönsted and Lewis acid sites appeared due to differently anchored MoO_3 species with support. Hence in order to understand the mechanism of transformation of weak acid sites in to strong acid sites, a survey of acid strength distribution was carried out and discussed in next section.

3.1.6. Pyridine adsorbed FT-IR

In order to obtain a clear distinction between Lewis and Brönsted acid sites FT-IR analysis of pyridine adsorbed on catalyst surface were carried out and results are displayed in Fig. 5. Pyridine adsorbed on Brönsted acid sites produce characteristic IR band around 1540 and 1638 cm^{-1} due vibration modes of adsorbed pyridine and bands at 1450 and 1480 cm^{-1} are assigned to pyridine coordinated with Lewis acid sites [41]. From Fig. 5 it can be seen that for sample MTS-5 bands are appeared at 1455, 1550 and 1639 cm^{-1} suggesting the presence of Brönsted as well as Lewis acid sites. But the greater intensity of band at 1455 cm^{-1} compared to other confirms the dominant presence of Brönsted acid over the surface of catalyst. Further for catalyst MTS-6, it was observed that the intensities of bands associated with Brönsted acidity decreases as compared to that of Lewis acidity. A similar trend was observed for MTS-7 catalyst but the intensities of the respective peaks are very low due to sharp decrease in the population of acid sites at high calcination temperature.

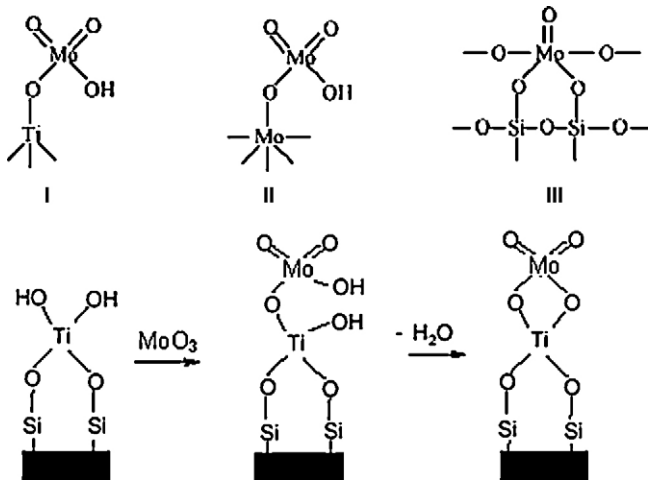

Scheme 1. Different MoO_3 species proposed to exist on TiO_2–SiO_2 support.

To know the sources of Lewis and Brönsted acid sites, one need to consider the way that MoO_3 species anchor to TiO_2–SiO_2 mixed oxide support. The most probable fittings of MoO_3 with support are shown in Scheme 1 and their relation with acidity is discussed further. At monolayer loading MoO_3 preferably reacts with TiO_2 hydroxyls mainly forming monodentate species I [42]. Such monodentate groups can also appears on the top of multilayers of amorphous Mo oxide forming species II. In literature, similar monodentate tetrahedral species were also proposed for MoO_3/Al_2O_3 and WoO_3/Al_2O_3 [43,44]. These monodentate species carry one proton (hydrogen) in their structures which act as a Brönsted acid center. On the other hand according to Zhao et al. [45] amorphous MoO_3 on SiO_2 is octahedrally coordinated species III and act as Lewis acid centers. From this point of view, catalyst calcined at 500 °C exhibited both Brönsted and Lewis acidity. Further, when catalyst is calcined at higher temperature (600 and 700 °C), hydroxyl groups from species I are removed in the form of water (shown separately in Scheme 1) due to which MoO_3 species on TiO_2 starts rearranging themselves forming species that corresponds to Lewis acidity. Moreover as observed by Liu et al. pure TiO_2 and SiO_2 show Lewis acidity and no acidity, respectively [40]. That is why the IR spectrum of pyridine adsorbed on MTS-6 and MTS-7 catalyst indicated the adverse effect of high calcination temperature on Brönsted acid site population over the catalyst surface.

3.2. Activity measurements

3.2.1. Nitration of phenol

The catalytic activities was tested for the nitration of phenol in the presence of mixed oxide supported MoO_3 catalyst using 30%

Table 2
Liquid phase batch process nitration of phenol over MTS series of catalysts.

Catalyst	Conversion of phenol (%)	Selectivity (%)			Total yield (%)	*o*/*p* ratio
		ONP	PNP	Benzq.		
Blank expt.	14	49	51	–	14	0.97
MTS-5	94	51	48	1	93	1.07
MTS-6	74	59	40	1	73	1.48
MTS-7	58	66	33	1	57	2.00

Operating conditions: phenol/HNO_3 = 1; catalyst = 1 g; HNO_3 = 30%; solvent = CCl_4; temperature: RT— reaction time: ~60 min. ONP = ortho-nitrophenol; PNP = para-nitrophenol; Benzq. = Benzoquinone. Total yield = ONP + PNP.

nitric acid at room temperature and the results are summarized in Table 2. Among the catalysts studied MTS-5 showed highest phenol conversion (94%) and 66% selectivity for *o*-nitrophenol was noted for MTS-7 catalyst. When the reaction was carried out without catalyst the conversion of phenol was low (14%) with nearly equal ortho- and para-isomers, suggests the influence of solid acid catalysts on the conversion and selectivity. To demonstrate the effect of calcination temperature, nitration is carried out with catalyst calcined at three different temperatures. No significant change in *o*-selectivity is observed when nitration was done using MTS-5 (calcined at 500 °C). This is due to occurrence of the reaction inside the larger pores of the catalyst in the same manner as in the bulk phase. This assumption is supported by the observation of closely similar distribution of products (*o*/*p* ratio) in the absence of catalyst. Nitration when performed using MTS-7, increase in *o*-nitrophenol selectivity was noted which may be because of preferred orientation of phenol inside the narrow pores increasing the accessibility of ortho-position to nitronium ion leading to selective formation of *o*-nitrophenol. Conversion (94%) of phenol in case of MTS-5 is attributed to the presence of more Brönsted acid sites over its surface. Such Brönsted acid sites are responsible for the generation of nitronium ion in the reaction [46]. When the catalyst is calcined at higher temperatures (MTS-6 and MTS-7) the number of Lewis acid sites increases which eventually decreases the Brönsted acid sites. Because of this reason the lowered conversion of phenol was observed when the nitration was performed with catalyst MTS-6 and MTS-7. 30% nitric acid limits the formation of di-nitrophenols and MTS series of catalysts are associated with very little or negligible formation of side product, generally which is benzoquinone.

3.2.2. Nitration of different aromatic substrates

Successful regioselective nitration of phenol has promoted us to extend the nitration studies to some other aromatic substrates. Hence, substrates like benzene, toluene and *o*-xylene were subjected to the nitration reaction and results are presented in Table 3. Exclusive formation of nitrobenzene, faster reaction rates and fairly good conversion of benzene are some of the advantages of carrying out the nitration of benzene with MTS series of catalyst. Though, the selectivity is not as much significant as in case of phenol nitration, the present method of nitration of toluene has advantage of suppression of polynitrated products. The lower selectivity in toluene nitration may be attributed to the weakly polar nature of the alkyl group which destabilizes any interaction with the catalyst leading to continue the reaction as like in the bulk phase. For MTS catalyzed *o*-xylene nitration conversions of *o*-xylene are also found low whereas selectivity did not alter considerably. Lowered conversions are mainly due to the formation of side products in the initial stage that deactivates the catalyst for further reaction.

In general, the change in conversion and selectivity of respective nitro-derivatives of these aromatic substrates can be well correlated to the change in the acidity and pore size distribution rather than to the change in the surface area of the catalysts.

3.2.3. Mechanism for nitration of phenol

Generally nitration requires aggressive mixture of acids (nitric and sulfuric acid) to generate NO_2^+, which is true nitrating intermediate. Brei et al. also explained that strong Brönsted acid sites are necessary for an effective formation of intermediate NO_2^+ ions from nitric acid [47]. Nitronium ion can be generated by the interaction of nitric acid with the Brönsted acid sites of solid acid catalyst. HNO_3 molecules when adsorbed on active Brönsted acid sites of catalyst, dissociates in to water, nitrate and nitronium ion. Because of electronegative hydroxyl group of phenol, the electron cloud of aromatic ring is pulled towards this group that makes ortho and para sites more favorable for NO_2^+ attack. During the propagation of such reaction steps, one H^+ ion is released out from aromatic substrate which recombines with the nitrate ions to form HNO_3 again. In this way reaction continues to form the nitrated aromatic compounds and generate water as a by-product. The plausible reaction mechanism for nitration of phenol over MTS series of catalyst is shown in Scheme 2.

3.2.4. Effect of Solvent

In order to search the best entariner, nitration of phenol over MTS-7 catalyst was performed using different solvents and their effect on phenol conversion and *o*-nitrophenol selectivity was studied. Fig. 6 clearly indicates that other solvents suffered with lower yields and *o*/*p* ratio where as chlorinated solvents showed the satisfactory results. Among them CCl_4 was found the best in all respects.

3.2.5. Effect of reaction time

Fig. 7 shows the influence of time on phenol nitration using MTS-7 catalyst. As seen in Fig., the conversion of phenol took place at a faster rate up to 40 min of reaction time and the saturation stage was reached in next 10 min. The faster reaction rate in the initial stage can be justified by the formation of more number of nitronium ions progressively in the reaction. *o*-Nitrophenol was the major product whereas para-nitrophenol form in fewer amounts. The selectivity towards *o*-nitrophenol does not affect significantly with increase in reaction time. Importantly, the increase in reaction time did not show the formation of any di-substituted nitrophenols.

3.2.6. Regeneration and reusability of the catalyst

After completion of the nitration of phenol over MTS-7 catalyst, it was filtered off and partly given wash with acetone and water and some part of spent catalyst was heated in an oven at 250 °C for 1 h. Thermal analysis of spent and regenerated catalyst was done

Table 3
Nitration of different aromatic substrates.

Aromatic substrate	Reaction conditions	Catalyst	Conversion (%)	Major products (selectivity, %)
Benzene	a	MTS-5	100	NB (100)
		MTS-6	91	NB (100)
		MTS-7	67	NB (99)
Toluene	b	MTS-5	82	ONT (48), PNT (46)
		MTS-6	69	ONT (42), PNT (57)
		MTS-7	35	ONT (40), PNT (59)
O-xylene	c	MTS-5	23	3-NOX (39), 4-NOX (44)
		MTS-6	14	3-NOX (33), 4-NOX (43)
		MTS-7	8	3-NOX (33), 4-NOX (42)

a: Catalyst: 0.1 g; benzene: 0.20 moles; nitric acid: 1 equivalent; temperature: room temperature; time: ~15 min. b: Catalyst: 1 g; toluene/HNO_3: 1.0; HNO_3: 69%; solvent: 1, 2-dichloroethane; temperature: reflux; time: ~60 min. c: Catalyst: 0.212 g (20% of o-xylene weight); o-xylene/HNO_3 mole ratio:1.0; HNO_3: 69%; solvent: carbon tetrachloride; temperature: 75 °C; time: ~90 min. NB: nitrobenzene; DNB: di-nitrobenzene. ONT: ortho-nitrotoluene; PNT: para-nitrotoluene; 3-NOX: 3-nitro-o-xylene; 4-NOX: 4-nitro-o-xylene.

Table 4
Comparison with various other solid acids under similar reaction conditions.

Catalyst	Conversion of phenol (%)	Selectivity (%)			*o*/*p* ratio	Ref.
		ONP	PNP	Benzq.		
$Fe/Mo/SiO_2$	60	48	42	10	1.14	[11]
H-ZSM-5	60	55	37	8	1.48	[11]
H-Y	60	60	30	10	2.00	[11]
MTS-5	94	51	48	1	1.07	This work
MTS-6	74	59	40	1	1.48	This work
MTS-7	58	66	33	1	2.00	This work

Operating conditions: phenol/HNO_3 = 1; catalyst = 1 g; HNO_3 = 30%; solvent = CCl_4; temperature: RT—reaction time: ~60 min. ONP = ortho-nitrophenol; PNP = para-nitrophenol; Benzq. = Benzoquinone.

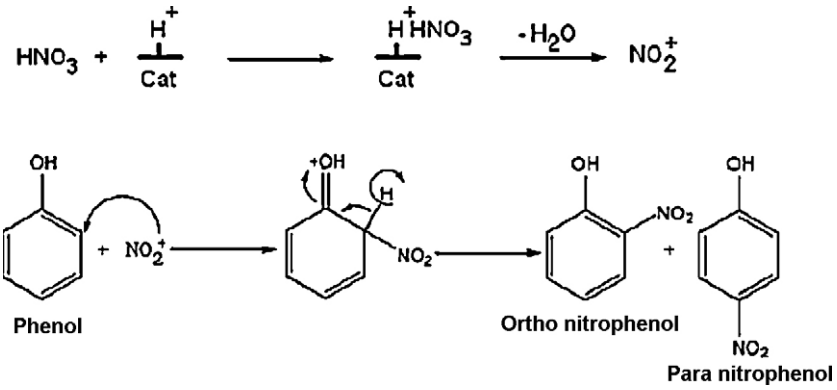

Scheme 2. The plausible reaction mechanism of nitration of phenol over MTS series of catalysts.

to ensure the amount of organic deposits over the catalyst surface. Study suggested acetone wash as the favorable method for regeneration of the catalyst. Catalyst regenerated by acetone wash when repeatedly used in the nitration of phenol, retained its activity for three cycles without affecting the o-nitrophenol selectivity. The 8% decrease in the yield (ONP + PNP) was observed, when catalyst used further in reaction.

3.2.7. Comparison

Under similar reaction conditions, the performance of MTS series of catalysts and other solid acids is compared for the nitration of phenol and the results are highlighted in Table 4. As could be noted, MTS-5 shows the best phenol conversion value among all solid acids and highest *o*/*p* nitrophenol ratio was observed for MTS-7 catalyst which is comparable to that of H-Y type of zeolites.

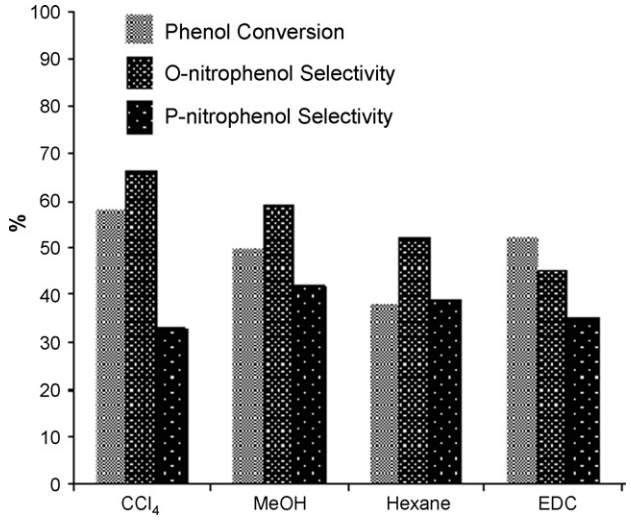

Fig. 6. Nitration of phenol over MTS-7 using different solvents.

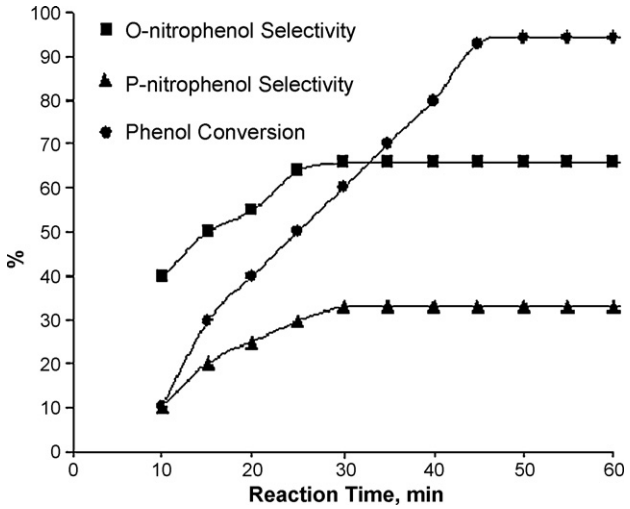

Fig. 7. Effect of reaction time on the catalytic activity.

But as H-Y zeolite suffers with large amount of side product (bezoqinone) formation, MTS-7 can be considered as the best agent in the respective process.

4. Conclusion

Following conclusions can be drawn from the results of nitration of phenol over MTS series of catalysts by using 30% nitric acid.

(1) MTS-7 catalyst is found suitable for nitration of phenol to achieve high ortho-nitrophenol yield at room temperature whereas MTS-5 gives very high phenol conversion.
(2) Progress in calcination temperature adversely affects the strength and acid amount of catalyst but change occur in porosity is suitable for ortho-nitrophenol yield.

(3) Activities of these catalysts are more related to nature of acid sites, acid amount and porosity of catalyst than surface area.
(4) In the process, no formation by-product and high *o*/*p* selectivity of catalysts at room temperature are some of the advantages.
(5) Avoid of sulfuric acid along with nitric acid used in diluted form makes the process safe and environmentally friendly.

References

[1] G.A. Olah, R. Malhotra, S.C. Narang, Nitration: Method and Mechanisms, VCH Publisher Inc., New York, 1989, pp. 201–204.
[2] A. Vogel, A Text Book of Practical Organic Chemistry, fourth ed., Longman, London, 1978, pp. 745–746.
[3] J.A.R. Rodrigues, A.P. de Oliveira Filho, P.J.S. Moran, R. Custodio, Tetrahedron 55 (1999) 6733–6738.
[4] S.M. Nagy, K.A. Yarovoy, M.M. Shakirov, V.G. Shubin, L.A. Vostrikova, K.G. Ione, J. Mol. Catal. 64 (1991) L 31–L 34.
[5] A. Cornelis, P.P. Laszlo, Synlett (1994) 155–161.
[6] M.J. Thompson, P.J. Zeegers, Tetrahedron 47 (1991) 8787–8790.
[7] T. Esakkidurai, K. Pitchumani, J. Mol. Catal. 185 (2002) 305–309.
[8] L.V. Malysheva, E.A. Paukshits, K.G. Ione, Catal. Rev. Sci. Eng. 37 (1995) 179–226.
[9] E. Suzuki, K. Tohmori, Y. Ono, Chem. Lett. 16 (1987) 2273–2274.
[10] K.M. Parida, P.K. Pattnaik, Catal. Lett. 47 (1997) 255–260.
[11] S.P. Dagade, V.S. Kadam, M.K. Dongare, Catal. Commun. 3 (2002) 67–70.
[12] M. Ouertani, P. Giraro, H.B. Kagan, Tetrahedron Lett. 23 (42) (1982) 4315–4318.
[13] H. Pervez, S.O. Onyisiuka, J.R. Rooney, C.J. Sukling, Tetrahedron 44 (1988) 4555–4565.
[14] D. Vanhove, S.R. Op, A. Fernandez, M. Blanchard, J. Catal. 57 (1979) 253–263.
[15] S. Okazaki, M. Kumasaka, J. Yoshida, K. Kosaka, K. Tanabe, Ind. Eng. Chem. Prod. Res. Div. 20 (1981) 301–305.
[16] K. Tanaka, K.I. Tanaka, J. Chem. Soc. Chem. Commun. (1984) 748–749.
[17] K. Segawa, T. Soeya, D.S. Kim, Res. Chem. Intermediat. 15 (1991) 129–151.
[18] L. Libetti, G. Ramis, G. Busca, F. Bregani, P. Forzatti, Catal. Today 61 (2000) 187–195.
[19] K. Aoki, M. Ohmae, T. Nanba, K. Takeishi, N. Azuma, A. Ueno, H. Ohfume, H. Hayashi, Y. Udagawa, Catal. Today 45 (1998) 29–33.
[20] Y. Liu, X. Ma, S. Wang, J. Gong, Appl. Catal. B 77 (2007) 125–134.
[21] S.B. Umbarkar, A.V. Biradar, S.M. Mathew, S.B. Shelke, K.M. Malshe, P.T. Patil, S.P. Dagde, S.P. Niphadkar, M.K. Dongre, et al., Green Chem. 8 (2006) 488–493.
[22] H. Hu, I.E. Waches, J. Phys. Chem. 99 (1995) 10911–10922, and references therein.
[23] M.S. Rana, S.K. Maity, J. Ancheyta, G. Murli Dhar, T.S.R. Prasada Rao, Appl. Catal. A 253 (2003) 165–176.
[24] S.K. Samantaray, K.M. Parida, Appl. Catal. A 211 (2001) 175–187.
[25] M.K. Kobayashi, R. Kuma, S. Masaki, N. Sugishima, Appl. Catal. B 60 (2005) 173–179.
[26] D. Mao, G. Lu, Q. Chen, Appl. Catal. A 263 (2004) 83–89.
[27] Y.C. Xie, Y.Q. Tang, Adv. Catal. 37 (1990) 1–43.
[28] S.R. Yoganarasimhan, C.N.R. Rao, Trans. Faraday Soc. 58 (1962) 1579–1589.
[29] M.M. Mohamed, T.M. Salama, T. Yamaguchi, Colloid Surf. A 207 (2002) 25–32.
[30] G.M.S. El Shafei, M.M. Mokhtar, Colloid Surf. A 94 (1995) 267–277.
[31] B.M. Reddy, B. Choddhury, J. Catal. 179 (1998) 413–419.
[32] X. Gao, I.E. Wachs, Catal. Today 51 (1999) 233–254.
[33] H. Kochkar, F. Figueras, J. Catal. 171 (1997) 420–430.
[34] R.A. Nyquist, C.L. Putzig, M.A. Leugers, Handbook of Infrared and Raman spectra of Inorganic Compounds and Organic Salts, Academic Press, New York, 1997, pp. 295–350.
[35] T. Fransen, P.C. Van Berge, P. Mars, in: B. Delmon, P.A. Jacobs, G. Poncelet (Eds.), Preparation of Catalysts, Elsevier, Amstardam, 1976, pp. 405–420.
[36] T. Gunji, Y. Nagao, T. Misono, Y. Abe, J. Non-Cryst. Solids 107 (1989) 149–154.
[37] F. Lonyl, J. Valyon, Micropor. Mesopor. Mater. 47 (2001) 293–301.
[38] M. Sawa, M. Niwa, Y. Murakami, Zeolites 10 (1990) 532–538.
[39] J. Ren, Z. Li, S. Liu, Y. Xing, K. Xie, Catal. Lett. 124 (2008) 185–194.
[40] Z. Liu, J. Tabora, R.J. Davis, J. Catal. 149 (1994) 117–126.
[41] A. Rahman, G. Lemay, A. Adnot, S. Kaliaguine, J. Catal. 112 (1988) 453–463.
[42] B.M. Reddy, et al., Appl. Catal. A 211 (2001) 19–30.
[43] C.A. Emis, J. Catal. 141 (1993) 347–354.
[44] J. Bernhole, H.A. Horsley, L.L. Murrell, J. Phys. Chem. 91 (1987) 1526–1530.
[45] B.Y. Zhao, Q. Xu, L.L. Gui, Y.Q. Tang, Acta Chim. Silica 48 (1990) 227–231.
[46] T. Mishra, Catal. Commun. 9 (2008) 21–26.
[47] V.V. Brei, S.V. Prudius, O.V. Melezhyk, Appl. Catal. A 239 (2003) 11–16.